Supporting information for:

On the atmospheric fate of methacrolein: 1. Peroxy radical isomerization following addition of OH and O_2

John D. Crounse,[*,†] Hasse C. Knap,[‡] Kristian B. Ørnsø,[‡] Solvejg Jørgensen,[‡] Fabien Paulot,[¶,§] Henrik G. Kjaergaard,[‡] and Paul O. Wennberg[*,†,¶]

Division of Geological and Planetary Science, California Institute of Technology, Pasadena, USA, 91125, Department of Chemistry, DK-2100 Copenhagen Ø, University of Copenhagen, Copenhagen, Denmark., and Division of Engineering and Applied Science, California Institute of Technology, Pasadena, USA, 91125

E-mail: crounjd@caltech.edu; wennberg@caltech.edu

Phone: 626-395-8655. Fax: 626-395-8535

[*]To whom correspondence should be addressed
[†]Division of Geological and Planetary Science, Caltech.
[‡]University of Copenhagen
[¶]Division of Engineering and Applied Science, Caltech.
[§]Now with the Division of Engineering and Applied Sciences, Harvard University, Cambridge, MA 02138, USA.

Calibrations

The chemical ionization signals for H_2O_2, methacrolein (MACR), and hydroxyacetone (HAC) were converted into mixing ratios using sensitivity factors determined from standard addition calibrations. Unfortunately, pure samples suitable for calibration are not available for MACR-1-OH-2-ONO_2, MACR-2-OH-1-ONO_2, MACR-1-OH-2-OOH, MACR-2-OH-1-OOH, and hydroperoxyacetone (HPAC). For these species, the CIMS sensitivities are estimated from the ion–molecule collision rate calculated using the parameterization of Su and Chesnavich.[S1] The conformationally-averaged dipole moment (weighted average of the dipoles for all conformers which contain $>1\%$ of the population at $T = 298$ K) and polarizability of the neutral molecule are needed for the collision rate calculation. These parameters are obtained using theoretical methods,[S2] and shown in Table S1.

The 2 addition of OH to MACR (MACR-2-OH-1-OO)

The addition of OH to the internal olefinic carbon of methacrolein (Scheme S1, channel c) has been estimated to account for $<9\%$ of the OH-reactivity.[S3,S4] Tuazon and Atkinson[S3] placed an upper bound on the yield of this channel using their determination of the methylglyoxal (MGLX) yield from the OH oxidation of methacrolein under high NO_x conditions, under the assumption that all the observed MGLX was produced from OH addition to the internal olefinic carbon. We propose that the hydroxy peroxy radical formed from OH addition to the internal olefinic carbon, MACR-2-OH-1-OO, will undergo a rapid 1,5-H-shift isomerization (similar to the 1,4-H-shift of MACR-1-OH-2-OO) followed by decomposition and reaction with O_2 to form hydroperoxyacetone (HPAC), CO, and HO_2 (see Scheme S1). This hypothesis is supported by theoretical calculations showing a low barrier ($\sim$13 kcal/mol above MACR-2-OH-1-OO) for the 1,5-H-shift reaction (Table S2).

CIMS signals observed at $m/z = 175$ are attributed to the CF_3O^- cluster with HPAC. The MSMS spectrum of this ion contains a daughter fragment ion with $m/z = 63$, a fragment which we have previously identified as a characteristic daughter ion (likely CFO_2^-) for hydroperoxide

Table S1: Conformationally averaged dipole moments and polarizibilities for methacrolein oxidation products, for $T = 298$ K. Collision rates have units of 10^{-9} cm^3 molec^{-1} s^{-1}.

		B3LYP/6-31G(d)		
Molecule	Structure	$\overline{\text{Dipole}}$ (D)	Polarizability (Å^3)	$k^{\text{x}}_{\text{coll}}$
MACR-1-OH-2-ONO$_2$	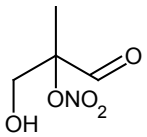	2.0	9.8	1.68
MACR-2-OH-1-ONO$_2$	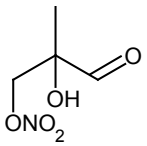	2.4	9.9	1.89
MACR-1-OH-2-OOH	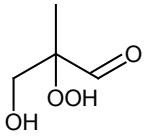	2.62	8.2	2.04
MACR-2-OH-1-OOH	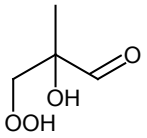	3.36	8.2	2.44
HAC	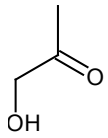	3.1	5.5	2.46
HPAC	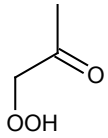	3.83	6.20	2.80

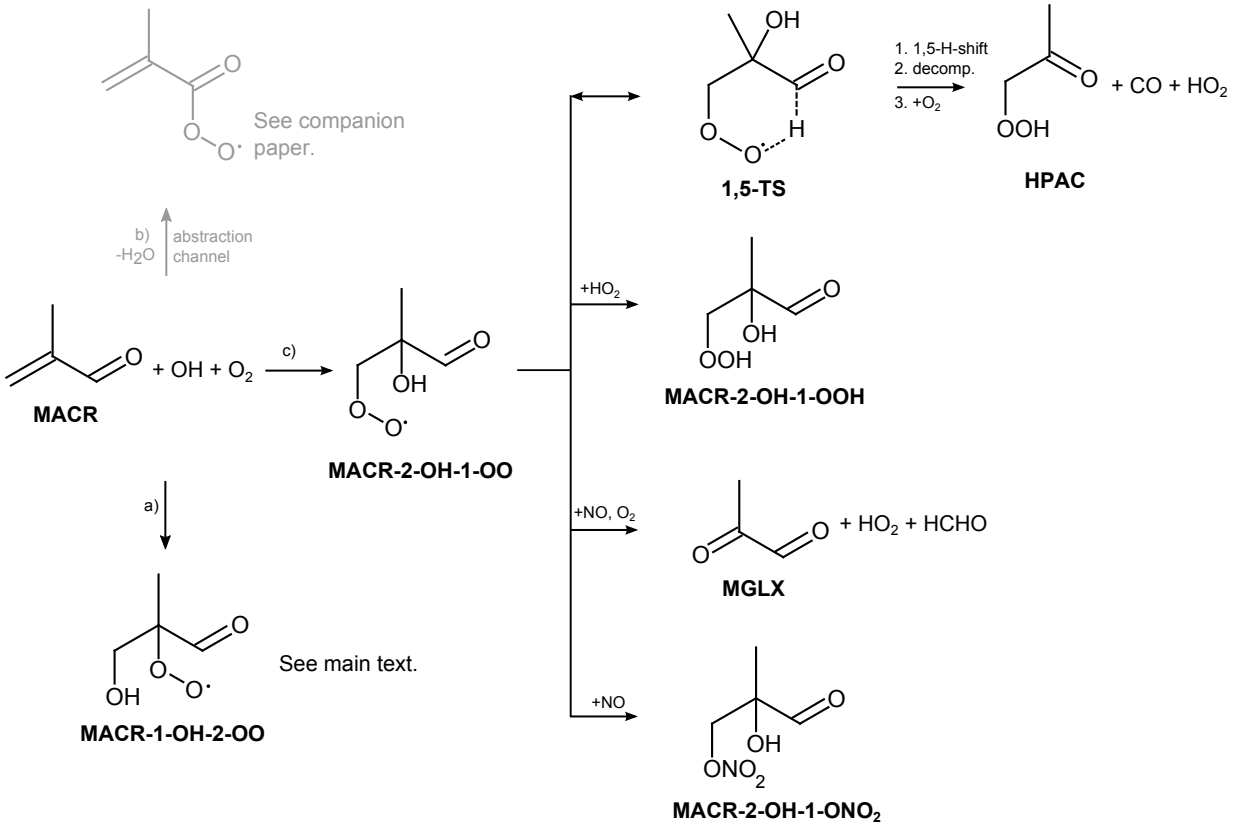

Scheme S1: Reaction channels and products for MACR-2-OH-1-OO peroxy radical.

species (ROOH).[S5,S6] In the ^{18}OH methacrolein oxidation experiment we observe both labeled and unlabeled HPAC, $CH_3C(^{18}O)CH_2OOH$ and $CH_3C(^{16}O)CH_2OOH$, respectively. The labeled versus unlabeled abundances for HPAC (HPAC-^{16}O:HPAC-^{18}O = 3.3:1) are very different from those of HAC (HAC-^{16}OH:HAC-^{18}OH = 1:2). We interpret this as evidence indicating that the bulk of HPAC formed in this experiment originates from a non-labeled channel, namely, the hydrogen abstraction channel. The ratio of HPAC-^{18}O:HAC-^{18}OH is 0.036±0.0033. Assuming the fate of both MACR-2-^{18}OH-1-OO and MACR-1-^{18}OH-2-OO is exclusive H-shift isomerization/decomposition to form HPAC-^{18}OH and HAC-^{18}OH, respectively, we estimate that $\frac{OH_{int}}{OH_{int}+OH_{ext}} = 0.035$.

The assumption that both hydroxy peroxy radicals react primarily through isomerization under these experimental conditions is supported through observations of very small yields for the hydroxy hydroperoxides (MACROOH, sum of MACR-1-OH-2-OOH and MACR-2-OH-1-OOH). We observe that [MACROOH]/[HAC]$<$0.05. A similar estimate for the fraction of OH addition occurring on the internal carbon is derived from the ratio of HPAC:HAC (0.031±0.0025) in the methylnitrite experiment with no initial NO. Here, HPAC formation from the hydrogen abstraction channel is suppressed due to preferential formation of MPAN.

Additional theoretical supporting information

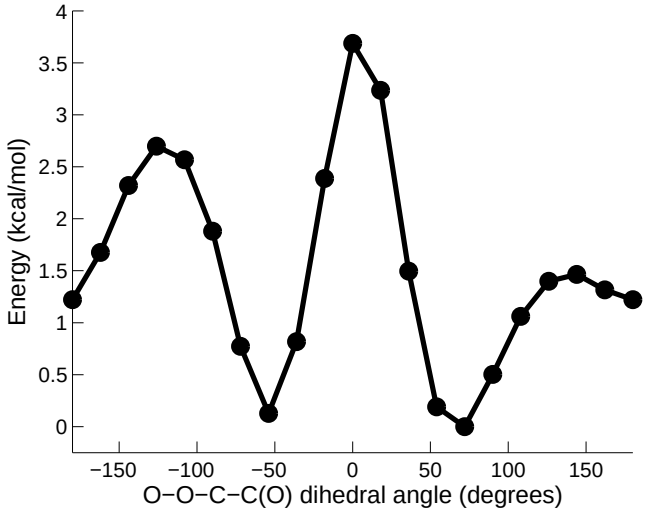

Figure S1: Optimized B3LYP/aug-cc-pVTZ energies as a function of (O)C-C-O-O dihedral angle in MACR-1-OH-2-OO.

Table S2: B3LYP/6-31+G(d,p) energetics of the 1,5-H-shift reaction for MACR-2-OH-1-OO for abstraction of aldehydic hydrogen atom (kcal/mol).

MACR + OH + O_2	0.0
MACR-2-OH-1-OO	-46.8
1,5-TS	-34.1
1,5-P	-43.1
HPAC + CO + HO_2 - O_2	-61.5

Table S3: Vibrational and rotational frequencies of the MACR-1-OH-2-OO reactant and transition states in the 1,4- and 1,5-H-shift reactions calculated with the B3LYP/aug-cc-pVTZ method and Opt=tight and Grid=ultrafine.

MACR-1-OH-2-OO		1,4-TS		1,5-TS	
$\widetilde{\nu}$ (cm^{-1})	B (GHz)	$\widetilde{\nu}$ (cm^{-1})	B (GHz)	$\widetilde{\nu}$ (cm^{-1})	B (GHz)
78.2	1.602	1716.6i	1.811	652.2i	1.710
97.6	1.853	97.5	1.884	80.5	1.867
146.2	2.363	135.3	2.189	133.4	2.489
188.1		157.7		189.5	
221.4		211.3		219.5	
249.6		235.5		277.0	
275.3		300.0		285.6	
336.3		319.1		310.7	
380.2		355.7		418.8	
431.7		456.6		470.5	
493.2		503.5		528.9	
525.7		567.2		597.4	
634.3		586.1		646.3	
762.6		630.2		671.7	
812.5		700.6		843.0	
886.7		830.9		890.1	
975.1		913.6		928.3	
1012.1		958.2		945.0	
1082.2		974.4		988.5	
1099.2		1081.7		1048.7	
1163.6		1089.3		1148.5	
1192.7		1131.4		1157.1	
1219.1		1157.1		1200.3	
1246.5		1211.9		1224.8	
1374.1		1254.7		1255.6	
1389.6		1366.4		1318.3	
1413.0		1410.4		1377.6	
1429.8		1437.8		1408.8	
1483.5		1481.2		1483.3	
1493.1		1493.1		1494.9	
1498.9		1497.1		1498.7	
1813.9		1784.3		1807.1	
2940.9		1942.9		1856.0	
2998.3		2986.1		2925.2	
3050.3		3048.0		2945.7	
3090.4		3078.7		2995.5	
3116.8		3114.9		3049.9	
3134.8		3129.2		3118.2	
3758.5		3718.9		3133.4	

Table S4: 1,4-H shift Transition State Theory (TST) reaction rates with Wigner[S7] and Eckart[S8] tunneling correction factors at different temperatures. The tunneling correction factors and uncorrected TST reaction rates are listed individually, along with the corrected TST reaction rates.

T (K)	TST (s^{-1})	Wigner	TST×Wigner (s^{-1})	Eckart	TST×Eckart (s^{-1})
250	5.61×10^{-5}	5.07	2.84×10^{-4}	1.73×10^{3}	9.68×10^{-2}
255	1.20×10^{-4}	4.91	5.88×10^{-4}	1.15×10^{3}	1.38×10^{-1}
260	2.48×10^{-4}	4.76	1.18×10^{-3}	7.90×10^{2}	1.96×10^{-1}
265	5.01×10^{-4}	4.62	2.32×10^{-3}	5.56×10^{2}	2.79×10^{-1}
270	9.86×10^{-4}	4.49	4.42×10^{-3}	4.00×10^{2}	3.94×10^{-1}
275	1.89×10^{-3}	4.36	8.25×10^{-3}	2.94×10^{2}	5.56×10^{-1}
280	3.55×10^{-3}	4.24	1.51×10^{-2}	2.20×10^{2}	7.82×10^{-1}
285	6.51×10^{-3}	4.13	2.69×10^{-2}	1.68×10^{2}	1.10×10^{0}
290	1.17×10^{-2}	4.02	4.71×10^{-2}	1.31×10^{2}	1.53×10^{0}
295	2.06×10^{-2}	3.92	8.08×10^{-2}	1.04×10^{2}	2.13×10^{0}
300	3.56×10^{-2}	3.82	1.36×10^{-1}	8.31×10^{1}	2.96×10^{0}
305	6.05×10^{-2}	3.73	2.26×10^{-1}	6.77×10^{1}	4.10×10^{0}
310	1.01×10^{-1}	3.64	3.69×10^{-1}	5.59×10^{1}	5.65×10^{0}
315	1.66×10^{-1}	3.56	5.92×10^{-1}	4.67×10^{1}	7.76×10^{0}
320	2.69×10^{-1}	3.48	9.36×10^{-1}	3.94×10^{1}	1.06×10^{1}
325	4.29×10^{-1}	3.41	1.46×10^{0}	3.37×10^{1}	1.45×10^{1}
330	6.74×10^{-1}	3.33	2.25×10^{0}	2.91×10^{1}	1.96×10^{1}
335	1.05×10^{-0}	3.26	3.42×10^{0}	2.53×10^{1}	2.65×10^{1}
340	1.60×10^{-0}	3.20	5.13×10^{0}	2.22×10^{1}	3.56×10^{1}
345	2.43×10^{-0}	3.14	7.61×10^{0}	1.97×10^{1}	4.77×10^{1}
350	3.63×10^{-0}	3.07	1.12×10^{1}	1.75×10^{1}	6.37×10^{1}

Table S5: 1,5-H shift Transition State Theory (TST) reaction rates with Wigner[S7] and Eckart[S8] tunneling correction factors at different temperatures. The correction factors are given both alone and multiplied with the TST rates. The tunneling correction factors and uncorrected TST reaction rates are listed individually, along with the corrected TST reaction rates.

T (K)	TST (s^{-1})	Wigner	TST×Wigner (s^{-1})	Eckart	TST×Eckart (s^{-1})
250	5.83×10^{-7}	1.59	9.26×10^{-7}	1.63	9.51×10^{-7}
255	1.35×10^{-6}	1.56	2.11×10^{-6}	1.60	2.16×10^{-6}
260	3.03×10^{-6}	1.54	4.67×10^{-6}	1.57	4.77×10^{-6}
265	6.59×10^{-6}	1.52	1.00×10^{-5}	1.55	1.02×10^{-5}
270	1.39×10^{-5}	1.50	2.09×10^{-5}	1.52	2.12×10^{-5}
275	2.87×10^{-5}	1.49	4.26×10^{-5}	1.50	4.31×10^{-5}
280	5.74×10^{-5}	1.47	8.43×10^{-5}	1.48	8.51×10^{-5}
285	1.12×10^{-4}	1.45	1.63×10^{-4}	1.46	1.64×10^{-4}
290	2.14×10^{-4}	1.44	3.08×10^{-4}	1.44	3.10×10^{-4}
295	4.02×10^{-4}	1.42	5.71×10^{-4}	1.43	5.73×10^{-4}
300	7.36×10^{-4}	1.41	1.04×10^{-3}	1.41	1.04×10^{-3}
305	1.32×10^{-3}	1.39	1.84×10^{-3}	1.40	1.84×10^{-3}
310	2.33×10^{-3}	1.38	3.22×10^{-3}	1.38	3.22×10^{-3}
315	4.03×10^{-3}	1.37	5.52×10^{-3}	1.37	5.51×10^{-3}
320	6.85×10^{-3}	1.36	9.31×10^{-3}	1.36	9.29×10^{-3}
325	1.15×10^{-2}	1.35	1.55×10^{-2}	1.34	1.54×10^{-2}
330	1.89×10^{-2}	1.34	2.53×10^{-2}	1.33	2.52×10^{-2}
335	3.07×10^{-2}	1.33	4.07×10^{-2}	1.32	4.06×10^{-2}
340	4.91×10^{-2}	1.32	6.47×10^{-2}	1.31	6.44×10^{-2}
345	7.76×10^{-2}	1.31	1.01×10^{-1}	1.30	1.01×10^{-1}
350	1.21×10^{-1}	1.30	1.57×10^{-1}	1.29	1.56×10^{-1}

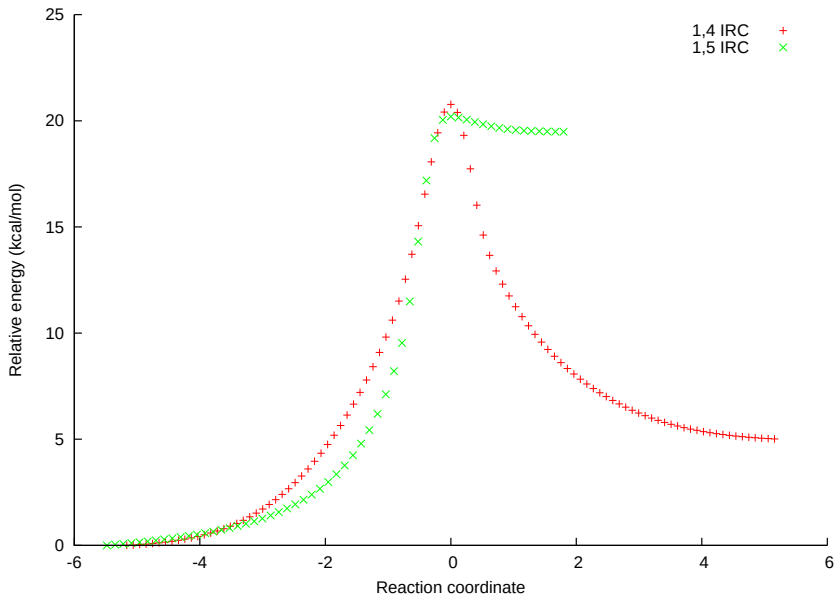

Figure S2: Molecular energies (kcal/mol) along the intrinsic reaction coordinate (IRC) for the 1,4- and 1,5-H-shift isomerization reactions of MACR-1-OH-2-OO calculated with B3LYP/aug-cc-pVTZ method.

References

(S1) Su, T.; Chesnavich, W. J. *J. Chem. Phys.* **1982**, *76*, 5183–5185.

(S2) Garden, A. L.; Paulot, F.; Crounse, J. D.; Maxwell-Cameron, I. J.; Wennberg, P. O.; Kjaergaard, H. G. *Chem. Phys. Lett.* **2009**, *474*, 45–50.

(S3) Tuazon, E. C.; Atkinson, R. *Int. J. Chem. Kinet.* **1990**, *22*, 591–602.

(S4) Orlando, J. J.; Tyndall, G. S.; Paulson, S. E. *Geophys. Res. Lett.* **1999**, *26*, 2191–2194.

(S5) Paulot, F.; Crounse, J. D.; Kjaergaard, H. G.; Kuerten, A.; St Clair, J. M.; Seinfeld, J. H.; Wennberg, P. O. *Science* **2009**, *325*, 730–733.

(S6) Crounse, J. D.; Paulot, F.; Kjaergaard, H. G.; Wennberg, P. O. *Phys. Chem. Chem. Phys.* **2011**, *13*, 13607–13613.

(S7) Wigner, E. *Phys. Rev.* **1932**, *40*, 0749–0759.

(S8) Eckart, C. *Phys. Rev.* **1930**, *35*, 1303–1309.